

# Stochastic background of gravitational waves generated by pre-galactic black holes

Eduardo S. Pereira<sup>\*</sup> and Oswaldo D. Miranda<sup>\*</sup>

*INPE – Instituto Nacional de Pesquisas Espaciais – Divisão de Astrofísica, Av. dos Astronautas 1758, São José dos Campos, 12227-010 SP, Brazil*

Accepted 2009 September 23. Received 2009 September 23; in original form 2009 March 19

## ABSTRACT

In this work, we consider the stochastic background of gravitational waves (SBGWs) produced by pre-galactic stars, which form black holes in scenarios of structure formation. The calculation is performed in the framework of hierarchical structure formation using a Press–Schechter-like formalism. Our model reproduces the observed star formation rate at redshifts  $z \lesssim 6.5$ . The signal predicted in this work is below the sensitivity of the first generation of detectors but could be detectable by the next generation of ground-based interferometers. Specifically, correlating two coincident advanced Laser Interferometer Gravitational-Wave Observatory (LIGO) detectors (LIGO III interferometers), the expected signal-to-noise ratio (S/N) could be as high as 90 (10) for stars forming at redshift  $z \simeq 20$  with a Salpeter initial mass function with slope  $x = 0.35$  (1.35), and if the efficiency of generation of gravitational waves, namely,  $\epsilon_{\text{GW}}$  is close to the maximum value  $\sim 7 \times 10^{-4}$ . However, the sensitivity of the future third generation of detectors as, for example, the European antenna EGO could be high enough to produce  $S/N > 3$  same with  $\epsilon_{\text{GW}} \sim 2 \times 10^{-5}$ . We also discuss what astrophysical information could be derived from a positive (or even negative) detection of the SBGWs investigated here.

**Key words:** black hole physics – gravitational waves – large-scale structure of Universe.

## 1 INTRODUCTION

Gravitational waves (GWs) are a natural consequence of Einstein’s theory of general relativity (GR). GWs will open a new astronomical window for the study of the Universe transforming the research in GR into an observational/theoretical study. In particular, the opening of the full electromagnetic spectrum to astronomical observation during the last century expanded our comprehension of the Universe. In this century, observations across the GW spectrum will provide a wealth of new knowledge, including the possibility of studying the period when the first stars were formed in the Universe at the end of the so-called ‘dark ages’.

The information provided by GWs is different when compared to that provided by electromagnetic waves. GWs carry detailed information on the coherent bulk motions of matter, such as those produced by the collapse of stellar cores generating, for example, black hole remnants. On the other hand, electromagnetic waves are usually an incoherent superposition of emissions from individual atoms, molecules and charged particles.

Because of the fact that GWs are produced by a large variety of astrophysical sources and cosmological phenomena, it is quite

probable that the Universe is pervaded by a background of such waves. Collapse of Populations II and III stars, phase transitions in the early Universe, cosmic strings and a variety of binary stars are examples of sources that could produce such a putative background of GWs (see e.g. Maggiore 2000; de Araujo, Miranda & Aguiar 2002, 2004; Sandick et al. 2006; Suwa et al. 2007a; Giovannini 2009 among others).

Note that the indirect evidence for the existence of GWs came first from observations of the orbital decay of the Hulse–Taylor binary pulsar (Hulse & Taylor 1974, 1975a,b). Direct detection though and analysis of GW sources are expected to provide a unique insight to one of the least understood of the fundamental forces (Belczynski, Kalogera & Bulik 2002). They will also allow us to investigate the physical properties of objects that do not emit any electromagnetic radiation as for example isolated black holes.

A number of interferometers designed for GW detection are currently in operation, being developed or planned. In particular, the high-frequency part of the GW spectrum ( $10 \lesssim f \lesssim 10^4$  Hz) is open today through the pioneering efforts of the first-generation ground-based interferometers such as Laser Interferometer Gravitational-Wave Observatory (LIGO). While detections from this first generation of detectors are likely to be rare, the advanced LIGO upgrade may detect, among others, the stochastic signal generated by a population of pre-galactic stars.

<sup>\*</sup>E-mail: duducosmo@das.inpe.br (ESP); oswaldo@das.inpe.br (ODM)

Thus, in the future, it may be possible to use GWs as a tool for studying the star formation at high redshifts. In particular, from the theoretical point of view, it can be found in the literature several works discussing this possibility. For example, the gravitational wave background (GWB) generated from the core collapse supernovae resulting in black holes at high redshifts has been discussed by Ferrari, Matarrese & Schneider (1999), de Araujo, Miranda & Aguiar (2000), de Araujo et al. (2004) among others. On the other hand, the calculation made specifically for Population III supernovae resulting in black holes is presented in de Araujo et al. (2002).

More recently, Sandick et al. (2006) calculated the GWB from Population III stars with the cosmic star formation history in the framework of hierarchical structure formation. On the other hand, Suwa et al. (2007a) presented the GWB spectrum of Population III stars by calculating the GW waveforms based on results of hydrodynamic core-collapsed simulations (see also Suwa et al. 2007b). It is worth stressing that in all of these works, one of the most important parameters responsible to characterize the GWB is the cosmic star formation rate (CSFR).

Concerning to the CSFR at high redshift, our knowledge is mainly based on numerical simulations performed by hydrodynamical codes in a  $\Lambda$  cold dark matter ( $\Lambda$ CDM) cosmology. Certainly, these simulations must reproduce the observable Universe at redshifts  $z \lesssim 6$ . In particular, the evidence for the existence of a large star formation at high redshift comes from, among others, the Gunn–Peterson effect (Gunn & Peterson 1965) and from the metallicity of  $\sim 10^{-2} Z_{\odot}$  found in high- $z$  Ly $\alpha$  forest clouds (Songaila & Cowie 1996; Ellison et al. 2000).

These results are consistent with a stellar population formed at  $z \gtrsim 5$  (Venkatesan 2000). However, measuring the CSFR from observations requires a number of assumptions, with the form of the dust obscuration corrections and the stellar initial mass function (IMF; Kroupa 2008; Wilkins, Trentham & Hopkins 2008).

Our main goal in the present paper is to discuss how the detection of a GWB could be used to give us some insight on the CSFR. This kind of study could also be used to constrain the fraction of massive stars that generates black holes at high redshift, and the efficiency of production of GWs by black holes whose distribution function is presently unknown. To do so, we use a hierarchical structure formation model similar to that developed by Daigne et al. (2006).

However, in our model the CSFR is obtained in a self-consistent way. That means, we solve the equation governing the total gas density taking into account the baryon accretion rate, treated as a infall term and the lifetime of the stars formed in the dark haloes.

The paper is organized as follows. In Section 2, we present the Press–Schechter (PS) like formalism used to determine the comoving abundance of collapsed dark matter haloes. In Section 3, we discuss how to obtain the CSFR from the hierarchical model. In Section 4, we present the formalism used to characterize the GWB. Section 5 presents our conclusions.

## 2 HIERARCHICAL FORMATION SCENARIO

PS heuristically derived a mass function for bound virialized objects in 1974 (Press & Schechter 1974). The basic idea of the PS approach is define haloes as concentrations of mass that have already left the linear regime by crossing the threshold  $\delta_c$  for non-linear collapse. Given a power spectrum and a window function, it should then be relatively straightforward to calculate the halo mass function as a function of the mass and redshift. However, it is worth stressing that the exact definition of the mass function, e.g. integrated versus differential form or count versus number density, varies widely in

the literature. To characterize different fits, it can be introduced the scale differential mass function  $f(\sigma, z)$  (Jenkins et al. 2001) defined as a fraction of the total mass per  $\ln \sigma^{-1}$  that belongs to haloes. That is,

$$f(\sigma, z) \equiv \frac{d\rho/\rho_B}{d \ln \sigma^{-1}} = \frac{M}{\rho_B(z)} \frac{dn(M, z)}{d \ln[\sigma^{-1}(M, z)]}, \quad (1)$$

where  $n(M, z)$  is the number density of haloes with mass  $M$ ,  $\rho_B(z)$  is the background density at redshift  $z$  and  $\sigma(M, z)$  is the variance of the linear density field. As pointed out by Jenkins et al. (2001), this definition of the mass function has the advantage that it does not explicitly depend on redshift, power spectrum or cosmology; all of these are contained in  $\sigma(M, z)$  (see also Lukić et al. 2007).

To calculate  $\sigma(M, z)$ , the power spectrum  $P(k)$  is smoothed with a spherical top-hat filter function of radius  $R$ , which on average encloses a mass  $M(R = [3M/4\pi\rho_B(z)]^{1/3})$ . Thus,

$$\sigma^2(M, z) = \frac{D^2(z)}{2\pi^2} \int_0^\infty k^2 P(k) W^2(k, M) dk, \quad (2)$$

where  $W(k, M)$  is the top-hat filter:

$$W(k, M) = \frac{3}{(kR)^3} [\sin(kR) - kR \cos(kR)], \quad (3)$$

and the redshift dependence enters only through the growth factor  $D(z)$ .

Then,

$$\sigma(M, z) = \sigma(M, 0)D(z). \quad (4)$$

In the more general case of a Universe with matter and a cosmological constant, the exact solution for the growth function is well approximated by (Carroll, Press & Turner 1992)

$$D(a) \approx \frac{5\Omega_m(a) a}{2 \left[ 1 - \Omega_\Lambda(a) + \Omega_m^{4/7} + (1/2)\Omega_m(a) \right]}, \quad (5)$$

where the relative density of the  $i$ -component is given by  $\Omega_i = \rho_i/\rho_c$ , and ‘ $i$ ’ applying for baryons (b), dark energy ( $\Lambda$ ) and total matter (m), while  $a = 1/(1+z)$  is the cosmological scale factor.

As usual, the primordial power spectrum is assumed to have a power-law dependence on scale, that is,  $P(k) \propto k^n$ . For a scale-invariant spectrum the spectral index is  $n = 1$ . The rate at which fluctuations grow on different scales is determined by an interplay between self-gravitation, pressure support and damping processes. These effects lead to a modification of the form of the primordial power spectrum that is expressed in terms of a transfer function  $T(k)$ . Thus, we have

$$P(k) = BkT(k), \quad (6)$$

where the normalization factor  $B$  is determined observationally.

For the transfer function, we consider (Efstathiou, Bond & White 1992)

$$T(k) = \frac{1}{\{1 + [ak + (bk)^{3/2} + (ck)^2]^v\}^{2/v}}, \quad (7)$$

with  $v = 1.13$ ,  $a = (6.4/\Gamma) h^{-1} \text{Mpc}$ ,  $b = (3.0/\Gamma) h^{-1} \text{Mpc}$ ,  $c = (1.7/\Gamma) h^{-1} \text{Mpc}$  and  $\Gamma = \Omega_m h e^{-\Omega_b(1+\sqrt{2h}/\Omega_m)}$  is the so-called shape parameter of the power spectrum (Bardeen et al. 1986; Peacock 1999).

We use throughout this work the mass function fit proposed by Sheth & Tormen (1999). That is,

$$f_{\text{ST}}(\sigma) = 0.3222 \sqrt{\frac{2a}{\pi}} \frac{\delta_c}{\sigma} \exp\left(-\frac{a\delta_c^2}{2\sigma^2}\right) \left[1 + \left(\frac{\sigma^2}{a\delta_c^2}\right)^p\right], \quad (8)$$

where  $a = 0.707$  and  $p = 0.3$ .

At redshift  $z$ , the comoving density of dark matter haloes in the mass range  $[M, M + dM]$  is  $f_{\text{ST}}(\sigma) dM$ , with (see, in particular, Daigne et al. 2006)

$$\rho_{\text{DM}} = \int_0^\infty f_{\text{ST}}(\sigma) M dM, \quad (9)$$

where  $\rho_{\text{DM}}$  is the comoving dark matter density.

We consider that the baryon distribution traces the dark matter distribution without bias. Thus, the density of baryons is proportional to the density of dark matter. The fact that stars can form only in structures that are suitably dense can be parametrized by the threshold mass  $M_{\text{min}}$ . Thus, the fraction of baryons at redshift  $z$  that are in structures is given by

$$f_b(z) = \frac{\int_{M_{\text{min}}}^{M_{\text{max}}} f_{\text{ST}}(\sigma) M dM}{\int_0^\infty f_{\text{ST}}(\sigma) M dM}. \quad (10)$$

With this definition, the baryon accretion rate  $a_b(t)$  which accounts for the increase in the fraction of baryons in structures is given by (Daigne et al. 2006)

$$a_b(t) = \Omega_b \rho_c \left( \frac{dt}{dz} \right)^{-1} \left| \frac{df_b(z)}{dz} \right|, \quad (11)$$

where  $\rho_c = 3H_0^2/8\pi G$  is the critical density of the Universe.

The age of the Universe that appears in (11) is related to the redshift by

$$\frac{dt}{dz} = \frac{9.78 h^{-1} \text{Gyr}}{(1+z)\sqrt{\Omega_\Lambda + \Omega_m(1+z)^3}}. \quad (12)$$

In equation (10) we have used as upper limit  $M_{\text{max}} = 10^{18} M_\odot$ . This choice permits a reasonable computational time to run the models. Moreover, models with  $M_{\text{max}} = 10^{24} M_\odot$  showed no considerable difference in the results. In the next section, we discuss how to obtain the CSFR from the hierarchical scenario here described.

### 3 THE COSMIC STAR FORMATION

In hierarchical models for galaxy formation the first star-forming haloes are predicted to collapse at redshift  $z \gtrsim 20$ , having masses  $\sim 10^6 M_\odot$  (Salvadori, Schneider & Ferrara 2007). In particular, the star formation history for a ‘galactic-like system’ is determined by the interplay between incorporation of baryons into collapsed objects (stars, stellar remnants and smaller objects) and return of baryons into diffuse state (gaseous clouds and intercloud medium of the system).

The later process can be twofold: (a) mass return from stars to the ‘interstellar medium of the system’ through, for example, stellar winds, and supernovae, which happens at the local level; (b) net global infall of baryons from outside of the system. The former process is a well known and firmly established part of the standard stellar evolution lore (see e.g. Chiosi & Maeder 1986), and although details of mass loss in a particular stellar type may still be controversial, there is nothing controversial in the basic physics of this process.

Thus, we use throughout this paper the basic process above described. To do that, we consider the baryon accretion rate  $a_b(t)$ , described by equation (11), as an infall term that supplies the reservoir represented by the haloes. Therefore, the number of stars formed by unity of volume, mass and time is given by

$$\frac{d^3 N}{dV dm dt} = \Phi(m)\Psi(t), \quad (13)$$

where  $\Phi(m)$  is the IMF which gives the distribution function of stellar masses, and  $\Psi(t)$  is the star formation rate. See that  $\Psi(t)$  is assumed to be independent of mass while  $\Phi(m)$  is assumed to be independent of time.

We use a Schmidt law (Schmidt 1959, 1963) for  $\Psi(t)$ . Therefore,

$$\frac{d^2 M_\star}{dV dt} = \Psi(t) = k[\rho_g(t)]^\alpha, \quad (14)$$

where  $k$  is a constant that will be identified later,  $\rho_g$  is the local gas density and  $\alpha = 1$ . See that (14) shows that stars are formed by the gas contained in the haloes.

On the other hand, we assume that the IMF follows the Salpeter (1955) form

$$\Phi(m) = Am^{-(1+x)}, \quad (15)$$

where  $x = 1.35$  (our fiducial value) and  $A$  is a normalization factor.

The constant  $A$  is determined by the condition which all stars are formed into the mass range  $[m_{\text{inf}}, m_{\text{sup}}]$ . That is,

$$\int_{m_{\text{inf}}}^{m_{\text{sup}}} Am^{-(1+x)} m dm = 1, \quad (16)$$

and we consider  $m_{\text{inf}} = 0.1 M_\odot$  and  $m_{\text{sup}} = 140 M_\odot$  as limits in (16).

The mass ejected from stars, for example through winds and supernovae, is returned to the ‘interstellar medium of the system’. Thus, we have

$$\frac{d^2 M_{\text{ej}}}{dV dt} = \int_{m(t)}^{m_{\text{sup}}} (m - m_r)\Phi(m)\Psi(t - \tau_m) dm, \quad (17)$$

where the lower limit of the integral,  $m(t)$ , corresponds to the stellar mass whose lifetime is equal to  $t$ . In the integrand,  $m_r$  is the mass of the remnant, which depends on the progenitor mass, and the star formation rate is taken at the retarded time  $(t - \tau_m)$ , where  $\tau_m$  is the lifetime of a star of mass  $m$ .

For all stars formed in the haloes, we use the metallicity-independent fit of Scalo (1986) and Copi (1997):

$$\log_{10}(\tau_m) = 10.0 - 3.6 \log_{10} \left( \frac{M}{M_\odot} \right) + \left[ \log_{10} \left( \frac{M}{M_\odot} \right) \right]^2, \quad (18)$$

where  $\tau_m$  is the stellar lifetime given in years.

The mass of the remnant,  $m_r$ , in equation (17) is calculated using the following assumptions.

(a) Stars with  $m < 1 M_\odot$  have a high lifetime so they do not contribute for  $M_{\text{ej}}$ .

(b) Stars with  $1 \leq m \leq 8 M_\odot$  after evolving off the main sequence left carbon–oxygen white dwarfs as remnants, where

$$m_r = 0.1156 m + 0.4551. \quad (19)$$

(c) Stars in the range  $8 < m \leq 10 M_\odot$  after evolving off the main sequence left oxygen–neon–magnesium white dwarfs with  $m_r = 1.35 M_\odot$ .

(d) Stars with  $10 < m < 25 M_\odot$  explode as supernovae leaving neutron stars as remnants ( $m_r = 1.4 M_\odot$ ).

(e) Stars with  $25 \leq m \leq 140 M_\odot$  produce black hole remnants. In this case, we consider that  $m_r = m_{\text{He}}$ . Note that  $m_{\text{He}}$  is the mass of the helium core before collapse (see Heger & Woosley 2002). Thus,

$$m_r = m_{\text{He}} = \frac{13}{24}(m - 20 M_\odot). \quad (20)$$

Then, using equations (14) and (17) we can write an equation governing the total gas density ( $\rho_g$ ) in the haloes. Namely,

$$\dot{\rho}_g = -\frac{d^2 M_\star}{dV dt} + \frac{d^2 M_{ej}}{dV dt} + a_b(t), \quad (21)$$

where  $a_b(t)$ , equation (11), gives the rate at which the haloes accrete mass.

Numerical integration of (21) produces the function  $\rho_g(t)$  at each time  $t$  (or redshift  $z$ ). Once obtained  $\rho_g(t)$ , we return to equation (14) in order to obtain the CSFR  $\Psi(t)$ . Just replacing  $\Psi(t)$  by  $\dot{\rho}_\star$  we can write

$$\dot{\rho}_\star = k\rho_g, \quad (22)$$

where the constant  $k$  represents the inverse of the time-scale for star formation. Namely,  $k = 1/\tau_s$ .

We normalize the CSFR in order to produce  $\dot{\rho}_\star = 0.016 M_\odot \text{ yr}^{-1} \text{ Mpc}^{-3}$  at  $z = 0$ . With this normalization, we obtain a good agreement with both the present value of the CSFR derived by Springel & Hernquist (2003), who employed hydrodynamic simulations of structure formation, and the observational points taken from Hopkins (2004, 2007).

The cosmological parameters used in our models are  $\Omega_\Lambda = 0.76$ ,  $\Omega_m = 0.24$ ,  $\Omega_b = 0.04$ ,  $\sigma_8 = 0.84$  and Hubble constant  $H_0 = 100 h \text{ km s}^{-1} \text{ Mpc}^{-1}$  with  $h = 0.73$ .

In Fig. 1 we present the CSFR derived from our models in function of the threshold mass  $M_{\min}$  (see equation 10). We use an IMF with slope  $x = 1.35$ ,  $\tau_s = 2.0 \text{ Gyr}$  as time-scale for star formation, and we consider that stars start to form at redshift  $z_{\text{ini}} = 20$ . As can be seen, models with  $M_{\min} = 10^6 - 10^8 M_\odot$  have an excellent agreement with the observational CSFR at redshifts  $z \lesssim 6.5$ . See that the threshold mass  $M_{\min}$  act on the amplitude and the redshift ( $z_\star$ ) at which the amplitude of the CSFR is maximum.

The model with  $M_{\min} = 10^{10} M_\odot$  has a good agreement with data at  $z \lesssim 5$ . On the other hand, at higher redshifts ( $5 \lesssim z \lesssim 6.5$ ) this model does not agree very well with the observational points. In Fig. 1 we also included the CSFR derived by Springel & Hernquist (SH) for comparison. Although our models with  $M_{\min} = 10^6 - 10^8 M_\odot$  have an amplitude greater than that derived by SH we can observe that both, SH and our models, fit very well the observational data.

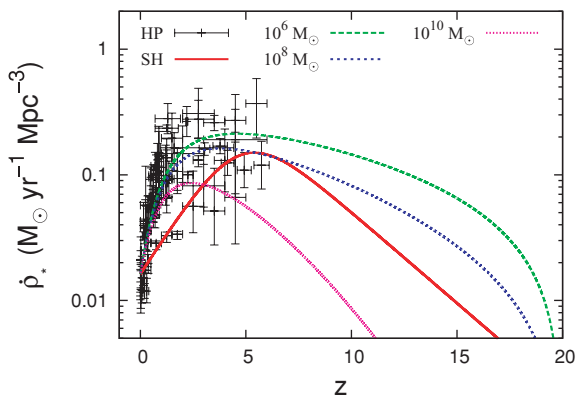


**Figure 1.** The CSFR obtained from our models compared to the observational points (HP) taken from Hopkins (2004), Hopkins (2007). We used a standard Salpeter IMF ( $x = 1.35$ ), and  $\tau_s = 2.0 \text{ Gyr}$  as time-scale for star formation. In this plot, we can see the influence of  $M_{\min}$  (the threshold mass for halo formation) on the CSFR. The solid line represents the SH CSFR, the dashed line corresponds to  $M_{\min} = 10^6 M_\odot$ , the short dashed line corresponds to  $M_{\min} = 10^8 M_\odot$  and the dotted line represents  $M_{\min} = 10^{10} M_\odot$ .

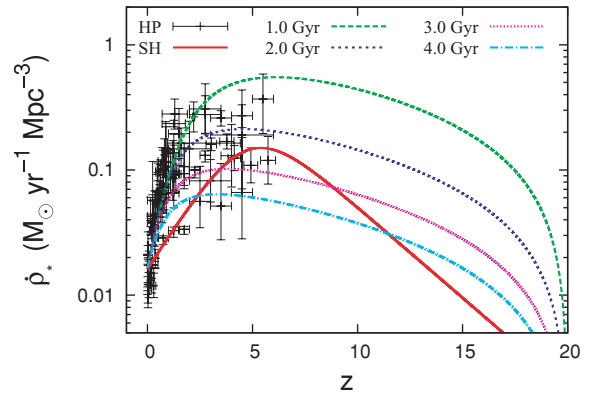


**Figure 2.** The influence of the time-scale for star formation ( $\tau_s$ ) on the results. The solid line represents the SH CSFR, the dashed line corresponds to  $\tau_s = 1.0 \text{ Gyr}$ , the short dashed line corresponds to  $\tau_s = 2.0 \text{ Gyr}$ , the dotted line corresponds to  $\tau_s = 3.0 \text{ Gyr}$  and the dot-dashed line represents  $\tau_s = 4.0 \text{ Gyr}$ . These models have a threshold mass  $M_{\min} = 10^6 M_\odot$ , and an IMF with slope  $x = 1.35$ . HP stands for the observational CSFR (Hopkins 2004, 2007).

In Fig. 2 we show the influence of  $\tau_s$  on the CSFR. We consider  $x = 1.35$ ,  $z_{\text{ini}} = 20$ , and we take  $M_{\min} = 10^6 M_\odot$  for the threshold mass. Note that,  $\tau_s \leq 2.0 \text{ Gyr}$  produces a gas consumption time-scale compatible with early-type galaxies (de Freitas Pacheco 1997). Thus, the first basic effect of increasing  $\tau_s$  is to shift the peak of the CSFR to lower redshifts. That means, the higher the  $\tau_s$  parameter, the lower is the redshift where appears the peak of  $\dot{\rho}_\star$ . In particular, the peak of  $\dot{\rho}_\star$  is shifted from redshift 3.3 if  $\tau_s = 4.0 \text{ Gyr}$  to 6.1 if  $\tau_s = 1.0 \text{ Gyr}$ .

The parameter  $\tau_s$  is also related to the amplitude of  $\dot{\rho}_\star$  (see also equation 22). See that considering  $M_{\min} = 10^6 M_\odot$  then the models with  $\tau_s = 2.0 - 3.0 \text{ Gyr}$  are those that present the best concordance with the observational data. It is worth stressing that both parameters,  $M_{\min}$  and  $\tau_s$ , produce similar effects on the results. That is, they act on the amplitude of  $\dot{\rho}_\star$  and on the value of  $z_\star$ . In Fig. 2 is also included the CSFR derived by SH for comparison.

In Fig. 3 we see the influence of  $z_{\text{ini}}$  on the evolution of  $\dot{\rho}_\star$ . The models have similar evolution at  $z \lesssim 5$ . However, at larger redshifts, the model with  $z_{\text{ini}} = 40$  produces a CSFR higher than that obtained

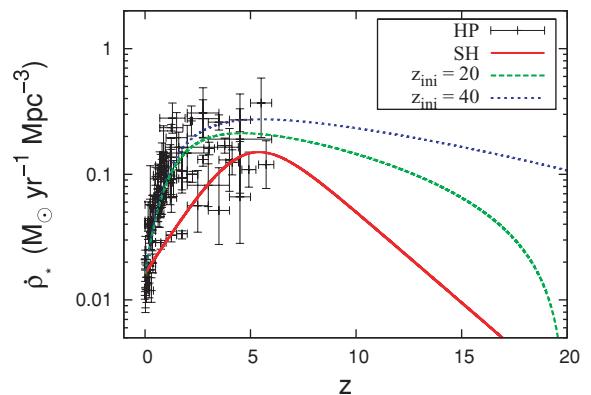


**Figure 3.** Models with  $\tau_s = 2.0 \text{ Gyr}$  and  $M_{\min} = 10^6 M_\odot$  but considering two different values for the initial redshift. The solid line corresponds to the SH CSFR, the dashed line corresponds to  $z_{\text{ini}} = 20$  and the short dashed line corresponds to  $z_{\text{ini}} = 40$ . HP stands for the observational CSFR (Hopkins 2004, 2007).

from  $z_{\text{ini}} = 20$ . In particular, the peak of the CSFR occurs at redshift 4.6 (5.5) for the model with  $z_{\text{ini}} = 20$  ( $z_{\text{ini}} = 40$ ).

It is worth stressing that the CSFR is inferred from observations of the light emitted by stars at various wavelengths. These observable samples are flux limited, and thus the intrinsic luminosity of the faintest objects in the sample changes with redshift. This incompleteness of the samples is corrected by using a functional (Schechter function) to the luminosity function obtained from the observations themselves.

An important parameter on the determination of the CSFR is the obscuration by dust that is well known to affect measurements of galaxy luminosity at ultraviolet (UV) and optical wavelengths. Correcting for this effect is not always straightforward. Thus, there are large uncertainties associated to the determination of the CSFR as can be seen from Figs 1–3 (see, in particular, Hopkins 2004; de Araujo & Miranda 2005 who discuss these uncertainties with more details).

#### 4 THE STOCHASTIC BACKGROUND OF GRAVITATIONAL WAVES

In this section we use the CSFR ( $\dot{\rho}_*$ ) obtained from the hierarchical model to determine the stochastic background of gravitational waves (SBGWs) generated by stars which collapse to black holes. Initially, we present a quick overview on the formalism used to characterize a SBGWs because this subject is discussed in previous works (see, for example, de Araujo et al. 2000, 2002, 2004; Miranda, de Araujo & Aguiar 2004; de Araujo & Miranda 2005). After this quick overview we display and compare the results of the models considered.

Let us write the specific flux received in GWs at the present epoch as

$$F_\nu(\nu_{\text{obs}}) = \int \frac{l_\nu}{4\pi d_L^2} \frac{d\nu}{d\nu_{\text{obs}}} dV, \quad (23)$$

where

$$l_\nu = \frac{dL_\nu}{dV} \quad (24)$$

is the comoving specific luminosity density (given e.g. in  $\text{erg s}^{-1} \text{Hz}^{-1} \text{Mpc}^{-3}$ ), which obviously refers to the source frame. See that  $dV$  is the comoving volume element, and  $d_L$  is the luminosity distance.

The above equations are valid to estimate a stochastic background radiation received on Earth independent of its origin. In the present paper  $l_\nu$  can be written as follows:

$$l_\nu = \int \frac{dE_{\text{GW}}}{d\nu} \dot{\rho}_*(z) \Phi(m) dm, \quad (25)$$

where  $dE_{\text{GW}}/d\nu$  is the specific energy of the source. Note that in the above equation  $\dot{\rho}_*(z)$  is the CSFR, and  $\Phi(m)$  is the IMF.

Thus, the flux  $F_\nu(\nu_{\text{obs}})$  received on Earth reads

$$F_\nu(\nu_{\text{obs}}) = \int \frac{1}{4\pi d_L^2} \frac{dE_{\text{GW}}}{d\nu} \frac{d\nu}{d\nu_{\text{obs}}} \dot{\rho}_*(z) \Phi(m) dm dV. \quad (26)$$

In particular, one can write the differential rate of production of GWs, for the case of a background produced by an ensemble of black holes, as follows:

$$dR_{\text{BH}} = \dot{\rho}_* \frac{dV}{dz} \Phi(m) dm dz. \quad (27)$$

Using equation (27) it follows that

$$F_\nu(\nu_{\text{obs}}) = \int \frac{1}{4\pi d_L^2} \frac{dE_{\text{GW}}}{d\nu} \frac{d\nu}{d\nu_{\text{obs}}} dR_{\text{BH}}. \quad (28)$$

Note that in the above equation, what multiplies  $dR_{\text{BH}}$  is nothing but the specific energy flux per unity frequency (in e.g.  $\text{erg cm}^{-2} \text{Hz}^{-1}$ ), i.e.

$$f_\nu(\nu_{\text{obs}}) = \frac{1}{4\pi d_L^2} \frac{dE_{\text{GW}}}{d\nu} \frac{d\nu}{d\nu_{\text{obs}}}. \quad (29)$$

On the other hand, the specific energy flux per unit frequency for GWs is given by (Carr 1980)

$$f_\nu(\nu_{\text{obs}}) = \frac{\pi c^3}{2G} h_{\text{BH}}^2. \quad (30)$$

Also, the spectral energy density, the flux of GWs, received on Earth,  $F_\nu$ , in  $\text{erg cm}^{-2} \text{s}^{-1} \text{Hz}^{-1}$  can be written as

$$F_\nu(\nu_{\text{obs}}) = \frac{\pi c^3}{2G} h_{\text{BG}}^2 \nu_{\text{obs}}. \quad (31)$$

From the above equations one obtains

$$h_{\text{BG}}^2 = \frac{1}{\nu_{\text{obs}}} \int h_{\text{BH}}^2 dR_{\text{BH}}. \quad (32)$$

See that  $h_{\text{BH}}$  is the dimensionless amplitude produced by the collapse of a star to form a black hole. Its expression is obtained from Thorne (1987). Thus,

$$h_{\text{BH}} \simeq 7.4 \times 10^{-20} \epsilon_{\text{GW}}^{1/2} \left( \frac{m_r}{M_\odot} \right) \left( \frac{d_L}{1 \text{ Mpc}} \right)^{-1}, \quad (33)$$

where  $\epsilon_{\text{GW}}$  is the efficiency of generation of GW's, and  $m_r$  is the mass of the black hole formed.

It is worth mentioning that equation (33) refers to the black hole ‘ringing’, which has to do with the de-excitation of the black hole quasi-normal modes.

The collapse of a star to black hole produces a signal with frequency  $\nu_{\text{obs}}$  given by

$$\nu_{\text{obs}} \simeq 1.3 \times 10^4 \text{ Hz} \left( \frac{M_\odot}{m_r} \right) (1+z)^{-1}, \quad (34)$$

where the factor  $(1+z)^{-1}$  takes into account the redshift effect on the emission frequency. That is, a signal emitted at frequency  $\nu_e$  at redshift  $z$  is observed at frequency  $\nu_{\text{obs}} = \nu_e(1+z)^{-1}$ .

As discussed in the previous section, we consider that black holes are formed from stars with  $25 \leq m \leq 140 M_\odot$ . The mass of the remnant is taken to be the mass of the helium core before collapse (see equation 20).

Another relevant physical quantity associated with the SBGWs is the closure energy density per logarithmic frequency span, which is given by

$$\Omega_{\text{GW}} = \frac{1}{\rho_c} \frac{d\rho_{\text{GW}}}{d \log \nu_{\text{obs}}}. \quad (35)$$

The above equation can be rewritten as

$$\Omega_{\text{GW}} = \frac{\nu_{\text{obs}}}{c^3 \rho_c} F_\nu = \frac{4\pi^2}{3H_0^2} \nu_{\text{obs}}^2 h_{\text{BG}}^2. \quad (36)$$

Thus, given a star formation history, consisting of a star formation rate per comoving volume (CSFR),  $\dot{\rho}_*(z)$ , and an IMF,  $\Phi(m)$ , the SBGWs produced by pre-galactic black holes can be characterize.

Finally, to assess the detectability of a GW signal, one must evaluate the signal-to-noise ratio (S/N), which for a pair of interferometers is given by (see e.g. Christensen 1992; Flanagan 1993; Allen 1997; de Araujo et al. 2002, 2004; Regimbau & de Freitas Pacheco 2006)

$$(S/N)^2 = \left[ \left( \frac{9H_0^4}{50\pi^4} \right) T \int_0^\infty d\nu \frac{\gamma^2(\nu) \Omega_{\text{GW}}^2(\nu)}{\nu^6 S_h^{(1)}(\nu) S_h^{(2)}(\nu)} \right], \quad (37)$$

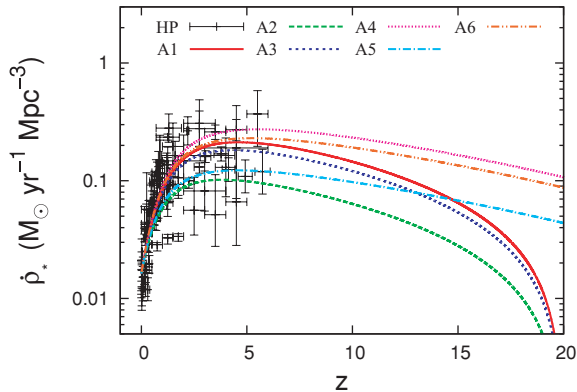


**Figure 4.** The CSFR for models with  $M_{\min} = 10^6 M_\odot$  and good agreement with observational data. The main characteristics of these models are described in Table 1.

where  $S_h^{(i)}$  is the spectral noise density,  $T$  is the integration time and  $\gamma(\nu)$  is the overlap reduction function, which depends on the relative positions and orientations of the two interferometers. For the  $\gamma(\nu)$  function we refer the reader to Flanagan (1993) who was the first to calculate a closed form for the LIGO observatories.

Using the formalism described above and in the previous sections we study a total number of 72 models varying the following parameters:

- the threshold mass ( $M_{\min}$ ) for structure formation, where we consider the values  $10^6$ ,  $10^8$  and  $10^{10} M_\odot$ ;
- the exponent ( $x$ ) of the IMF, where we consider  $x = 1.35$  (‘Salpeter exponent’),  $x = 0.35$  which yields a higher number of black hole remnants than Salpeter IMF and  $x = 2.35$  which produces a lower number of black hole remnants than Salpeter exponent;
- the time-scale for star formation ( $\tau_s$ ), where we consider the values 1.0, 2.0, 3.0 and 4.0 Gyr;
- the initial redshift ( $z_{\text{ini}}$ ) where star formation begins to occur. We take the values 20 and 40.

On this set of models we use two criteria for selecting the best ones. The first criterion is to have good agreement with observational star formation data at redshifts  $z \lesssim 6.5$ .<sup>1</sup> The second criterion is to produce a  $S/N > 3$  for a pair of ‘advanced’ interferometers. We consider this choice of  $S/N$  as reasonable for an adequate characterization of the SBGWs.

Fig. 4 presents the models with  $M_{\min} = 10^6 M_\odot$  which satisfy the above criteria.

Table 1 shows the main results for the six models A1–A6 which are presented in Fig. 4. The efficiency of generation of GWs is taken from Stark & Piran (1986) who simulated the axisymmetric collapse of a rotating star to black hole. We use their maximum value, namely,  $\epsilon_{\text{GWmax}} = 7 \times 10^{-4}$ . We will discuss below the dependence of  $\epsilon_{\text{GW}}$  on the results.

See that to calculate the  $S/N$  we consider that the integration time in equation (37) is 1 yr. In the fifth column of Table 1 we present the redshift ( $z_*$ ) where the CSFR reaches its maximum value; in the sixth column we present the  $S/N$ .

<sup>1</sup> We performed  $\chi^2$  analysis over the models with  $S/N > 3$ . In particular, we determine the reduced  $\chi^2$  defined as  $\chi_r = \chi^2/\text{dof}$  (where ‘dof’ means ‘degrees of freedom’). We consider that models with  $\chi_r \leq 1$  have good agreement with observational data.

**Table 1.** The main results of the models with  $M_{\min} = 10^6 M_\odot$  of the Fig. 4. The  $S/N$  is presented for a pair of LIGO III (advanced configuration) interferometers.  $S/N$  is computed for 1 yr of observation and we consider a GW efficiency  $\epsilon_{\text{GWmax}} = 7 \times 10^{-4}$ .

Model	$z_{\text{ini}}$	$x$ (IMF)	$\tau_s$ (Gyr)	$z_*$	$S/N$
A1	20	1.35	2.0	4.6	7.4
A2	20	1.35	3.0	3.8	3.8
A3	20	0.35	1.0	4.4	93.5
A4	40	1.35	2.0	5.6	9.8
A5	40	1.35	3.0	4.6	4.8
A6	40	0.35	1.0	5.3	119.9

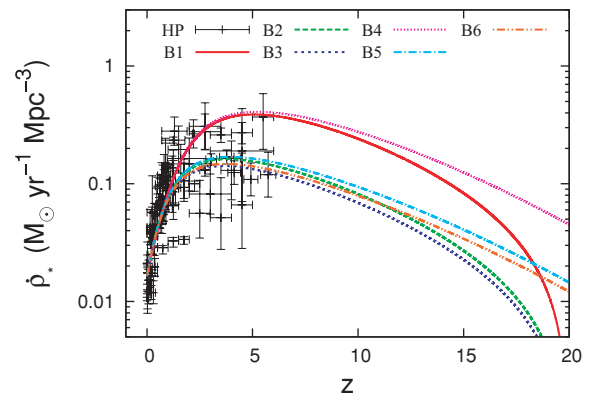


**Figure 5.** The CSFR for models with  $M_{\min} = 10^8 M_\odot$  and good agreement with observational data. The main characteristics of these models are described in Table 2.

Note that there is possibility of detecting the SBGWs here proposed if  $\epsilon_{\text{GW}}$  is around the maximum value. Observe that for Salpeter IMF ( $x = 1.35$ ) we obtain a significant  $S/N$  if  $\tau_s \sim 2.0$ – $3.0$  Gyr.

On the other hand, the models with  $x = 0.35$  produce the highest values for the  $S/N$ . This happens because  $x = 0.35$  produces a higher number of massive stars than the Salpeter IMF. In this case, the CSFR that fit the observational data are those with  $\tau_s \lesssim 1.0$  Gyr. See that the models with  $\tau_s \lesssim 1.0$  Gyr have a short time-scale for star formation. These values for the parameter  $\tau_s$  are consistent with a high-mass stellar population.

However, if the IMF of pre-galactic stars is close to  $x = 2.35$  then there is no hope of detecting the SBGWs we proposed here, even for ideal orientation and locations of the LIGO interferometers. In particular, all models with  $x = 2.35$  have  $S/N < 0.1$ , same for those models producing  $\dot{\rho}_*$  with excellent agreement with Hopkins data. Thus, the first conclusion is that it would be possible the detection of a background of pre-galactic black holes if the IMF of these objects is  $x \gtrsim 1.35$  and if  $\epsilon_{\text{GWmax}} \sim 7 \times 10^{-4}$ .

In order to see the influence of  $M_{\min}$  on the value of the  $S/N$  we present in Fig. 5 the models with  $M_{\min} = 10^8 M_\odot$  and that satisfy our two criteria as above defined.

Table 2 shows the main results for the six models B1–B6 which are presented in Fig. 5. The first effect of  $M_{\min}$  is to shift  $z_*$  (for example, compare models A1 and B2). That is, a halo with mass  $10^6 M_\odot$  collapses earlier than a halo with mass  $10^8 M_\odot$ . Thus, the maximum of star formation for models with  $10^8 M_\odot$  will be shifted to low redshifts.

The second effect is on the amplitude of  $\dot{\rho}_*$  as discussed in the previous section. As the quantity of black holes is  $\propto \dot{\rho}_*$  then

**Table 2.** The main results of the models with  $M_{\min} = 10^8 M_{\odot}$ .

Model	$z_{\text{ini}}$	$x$ (IMF)	$\tau_s$ (Gyr)	$z_{\star}$	S/N
B1	20	1.35	1.0	5.1	11.9
B2	20	1.35	2.0	3.8	5.7
B3	20	0.35	1.0	3.6	72.8
B4	40	1.35	1.0	5.2	13.2
B5	40	1.35	2.0	3.9	6.2
B6	40	0.35	1.0	3.8	77.6

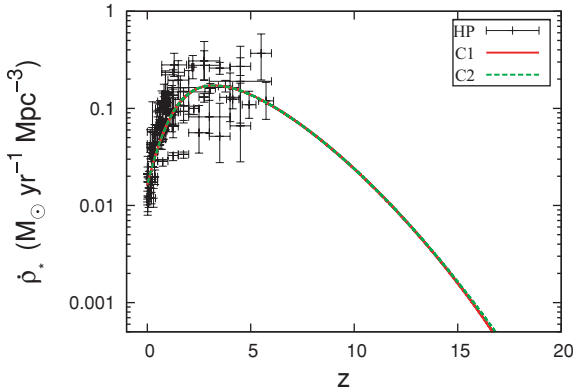
increasing the value of  $M_{\min}$  the number of black holes formed will decrease. As a consequence, models with  $10^8 M_{\odot}$  present a lower S/N than those with  $M_{\min} = 10^6 M_{\odot}$ .

The third effect can be seen comparing Tables 1 and 2. The models which satisfy the selection criteria with  $M_{\min} = 10^6 M_{\odot}$  are those with  $\tau_s \sim 2.0\text{--}3.0$  Gyr for  $x = 1.35$ . Otherwise, with  $M_{\min} = 10^8 M_{\odot}$  the selection criteria are satisfied if  $\tau_s \sim 1.0\text{--}2.0$  Gyr for  $x = 1.35$ . This result can be understood remembering that  $\tau_s$  also acts on the amplitude of  $\dot{\rho}_{\star}$ .

That means, if we decrease the value of  $\tau_s$  the amplitude of  $\dot{\rho}_{\star}$  increases (see, for an instance, Fig. 2 and equation 22). On the other hand, as above discussed, if we increase the parameter  $M_{\min}$ , the amplitude of  $\dot{\rho}_{\star}$  is reduced. Thus, if we change  $M_{\min}$  from  $10^6$  to  $10^8 M_{\odot}$ , we have to decrease the parameter  $\tau_s$  in order to obtain  $\dot{\rho}_{\star}$  with good agreement with the observational data and also to produce S/N > 3.

In Fig. 6 we present the models with  $M_{\min} = 10^{10} M_{\odot}$  (see details of the models in Table 3). Only those with  $x = 1.35$  and  $\tau_s = 1.0$  Gyr have a good agreement with observational data and produce S/N > 3. See that the difference between models C1 and C2 is very subtle.

This happens because the fraction of baryons in structures with  $M > 10^{10} M_{\odot}$  is very small at redshifts 20–40. Thus,  $z_{\text{ini}}$  does not have strong influence on the evolution of the models C1 and C2 at low redshifts.


**Figure 6.** The CSFR for models with  $M_{\min} = 10^{10} M_{\odot}$  and good agreement with observational data. The main characteristics of these models are described in Table 3.

**Table 3.** The main results of the models with  $M_{\min} = 10^{10} M_{\odot}$ .

Model	$z_{\text{ini}}$	$x$ (IMF)	$\tau_s$ (Gyr)	$z_{\star}$	S/N
C1	20	1.35	1.0	3.2	5.4
C2	40	1.35	1.0	3.2	5.6

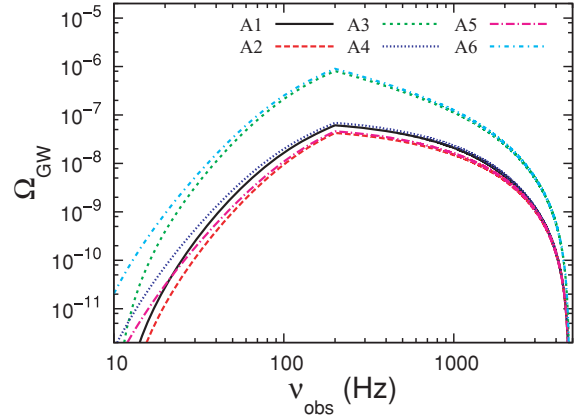

**Figure 7.** Spectrum of the gravitational energy density parameter  $\Omega_{\text{GW}}$ . Results are shown for the models A1–A6 of the Table 1.

Fig. 7 shows the density parameter  $\Omega_{\text{GW}}$  as a function of the observed frequency  $\nu_{\text{obs}}$ . The density parameter increases at low frequencies and it reaches a maximum amplitude of about  $9.0 \times 10^{-7}$  around 200 Hz in the model A6. On the other hand, model A2 reaches a maximum amplitude of  $4.2 \times 10^{-8}$  also around 200 Hz. See that both the maximum amplitude of  $\Omega_{\text{GW}}$  and the high-frequency part of the spectra<sup>3</sup> are not strongly dependent on the initial redshift  $z_{\text{ini}}$ . To verify that, compare the models A1 and A4, A2 and A5 and A3 and A6.

However, the value of  $z_{\text{ini}}$  has influence over the low-frequency part of the spectra as can be seen from Fig. 7. This part of the spectrum is dominated by the population of black holes formed at redshifts  $z \gtrsim 7$ .

It is worth stressing that de Araujo et al. (2004) assuming a SH (Springel & Hernquist 2003) model of star formation obtained a similar result for  $\Omega_{\text{GW}}$ . Their spectrum peaks at  $\Omega_{\text{GW}} h^2 \approx 5 \times 10^{-9}$  at  $\nu_{\text{obs}} \approx 200$  Hz for a Salpeter IMF. Using  $h = 0.73$  we find  $\Omega_{\text{GW}} \sim 9 \times 10^{-9}$  for their fiducial model.

This is a factor of  $\sim 5$  lower than the maximum amplitude of  $\Omega_{\text{GW}}$  obtained by our model A2. However, note that  $\dot{\rho}_{\star}$  obtained from ‘model 3.0 Gyr’ in Fig. 2, which corresponds to model A2 in Table 1, is smaller than the SH CSFR only in the range  $4.5 \lesssim z \lesssim 8.2$ . Thus, except for this interval in redshift, the rate of core collapse obtained from SH CSFR is actually smaller than that obtained from model A2.

The cusp in the curves shown in the Fig. 7 is produced by our choice to the energy flux (see equations 29 and 30). See that the closure energy density ( $\Omega_{\text{GW}}$ ) is directly proportional to the energy flux, and therefore more sensitive to its frequency dependence. Here, the specific energy flux is obtained from equation (33), which takes into account the most relevant quasi-normal modes of a rotating black hole.

In particular, we refer the reader to de Araujo et al. (2000) who discuss the formulation presented here and compare it to that used by Ferrari et al. (1999) where the energy flux is a function of frequency. Thus, their closure energy density is broader than we use here. As a consequence,  $\Omega_{\text{GW}}$  obtained by Ferrari et al. (1999) has a smoother

<sup>2</sup> The model A2 is that which has the smallest values for  $\Omega_{\text{GW}}$ . As a consequence, from all models presented in Tables 1–3, A2 is that which present the smallest S/N.

<sup>3</sup> Concerning for the results presented in Figs 7 and 8 we are defining the high-frequency part of the spectra as that for which  $\nu_{\text{obs}} > 200$  Hz.

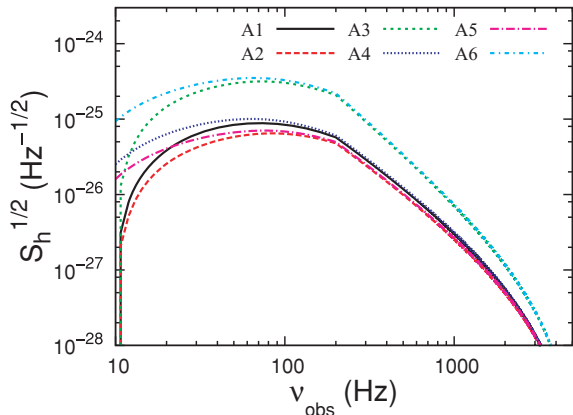


**Figure 8.** Gravitational strain in  $\text{Hz}^{-1/2}$ . Results are shown for the models A1–A6 of the Table 1.

peak than ours. However, as discussed in de Araujo et al. (2000), both formulations presented similar results.

Since some authors use, instead of  $\Omega_{\text{GW}}$ , the gravitational strain  $S_h^{1/2}$ , defined by Allen & Romano (1999) as

$$S_h = \frac{3H_0^2}{4\pi^2} \frac{1}{\nu_{\text{obs}}} \Omega_{\text{GW}}, \quad (38)$$

we show this quantity in Fig. 8.

A key parameter to determine the values presented in Tables 1–3 is the efficiency of generation of GWs. We take the maximum efficiency found by Stark & Piran (1986), namely,  $\epsilon_{\text{GW}_{\text{max}}} = 7 \times 10^{-4}$  for an axisymmetric collapse resulting in a black hole.

On the other hand, more recently, Fryer, Woosley & Heger (2001) obtained the efficiency of  $2 \times 10^{-5}$  for a  $100 M_{\odot}$  black hole remnant. Note that since  $\Omega_{\text{GW}} \propto \epsilon$ , if the efficiency is actually closer to  $2 \times 10^{-5}$ , the observed energy density in GWs may be divided by a factor of 35. In this case, of all models here studied only model A6 will produce  $S/N > 3$ .

However, the distribution of  $\epsilon_{\text{GW}}$  in function of the mass of a black hole is unknown. In particular, let us think of what occurs with other compact objects – namely, the neutron stars – to see if we can learn something from them. A newly born neutron star could lose angular momentum due to GWs associated with non-radial oscillations (Ferrari, Miniutti & Pons 2003). This could explain why all known young neutron stars are relatively slow rotators.

The black holes could have had a similar history, i.e. they could have been formed rapidly rotating and lost momentum to gravitational radiation via their quasi-normal modes. If this was the case, the value of  $\epsilon_{\text{GW}}$  could be near the maximum one, or in the worst case, it could have a value to produce  $S/N > 3$  for a LIGO III pair.

## 5 SUMMARY AND DISCUSSION

In this work, we have used the hierarchical formation scenario derived from the PS formalism to build the CSFR – in a self-consistent way. Our paper differs from earlier works basically in the form as is obtained from the function  $\dot{\rho}_*$  (or CSFR).

In particular, from the hierarchical scenario we obtain the baryon accretion rate,  $a_b(t)$ , that supplies the gaseous reservoir in the haloes. Thus, the term  $a_b(t)$  is treated as an infall term in our model.

This scenario is in agreement with the CDM model of cosmological structure formation, where the first sources of light are expected to form in  $\sim 10^6 M_{\odot}$  dark matter potential at  $z \geq 20$ .

Using  $\dot{\rho}_*$  we calculate the SBGWs produced by pre-galactic black holes. We show that a significant amount of GWs is produced related to the history of CSFR studied here, and this SBGWs can in principle be detected by a pair of LIGO III interferometers.

Note that  $S/N \sim 90$  could be obtained if the efficiency of generation of GWs is close to the maximum value ( $\epsilon_{\text{GW}_{\text{max}}} = 7 \times 10^{-4}$ ), if the IMF produces a high number of massive remnants ( $x = 0.35$ ), and if  $z_{\text{ini}} \sim 20$ . Considering a Salpeter IMF ( $x = 1.35$ ), we obtain  $S/N \sim 10$ .

The critical parameter to be constrained in the case of a non-detection is  $\epsilon_{\text{GW}}$ . A non-detection would mean that the efficiency of GWs during the formation of black holes is not high enough. In reality,  $\epsilon_{\text{GW}_{\text{max}}}$  should be divided by a factor of  $> 35$  in the case of a non-detection.

It is worth mentioning that an IMF with  $x = 2.35$  could also be responsible for a non-detection same with  $\epsilon_{\text{GW}} = \epsilon_{\text{GW}_{\text{max}}}$ . However,  $x = 2.35$  produces a high number of low-mass stars that is not in agreement with recent numerical simulations of the collapse and fragmentation of primordial clouds (see e.g. Abel, Bryan & Norman 2002).

Another possibility for a non-detection is that the pre-galactic stars are such that the black holes formed had masses  $> 500 M_{\odot}$ . In this case, the GW frequency band would be out of the LIGO bandwidth.

However, considering black holes formed from stars with masses  $25 \lesssim m \lesssim 140 M_{\odot}$ , then the sensitivity of the future third generation of detectors could be high enough to increase one order of magnitude in the expected value of  $S/N$ . Examples of such detectors are the Large-Scale Cryogenic Gravitational Wave Telescope (LCGT) and the European antenna EGO (see Regimbau & de Freitas Pacheco 2006 and the references therein for a short discussion on this subject).

Specifically, around 650 Hz the planned strain noise for EGO will be a factor of  $\sim 4$  higher than that provided for advanced LIGO configuration. This could represent a gain of a factor of  $\sim 5$ – $20$  for the value of  $S/N$  considering two interferometers located at the same place (see Regimbau & de Freitas Pacheco 2006). Thus, some models in Tables 1–3 could survive with  $S/N > 3$  same with  $\epsilon_{\text{GW}} \sim 2 \times 10^{-5}$ .

In particular, the detection of a background with significant  $S/N$  would permit us to obtain the curve  $S_h^{1/2}$  (or  $\Omega_{\text{GW}}$ ) versus  $\nu_{\text{obs}}$ . From it, one can constrain  $\dot{\rho}_*$  at high redshifts and the GW efficiency ( $\epsilon_{\text{GW}}$ ). Thus, the detection and characterization of a SBGWs could be used as a tool for study of the star formation at high redshifts.

It is worth stressing that several astrophysical sources can contribute to the background of GWs, as mentioned in the Introduction. In principle, it should be possible to distinguish different sources from the detected GW spectrum. That is, from the characteristics of the observed curve  $\Omega_{\text{GW}}$  versus  $\nu_{\text{obs}}$ .

For example, in the present work we have shown that cosmological stellar black holes ( $3 \lesssim M_{\text{BH}}/M_{\odot} \lesssim 65$ ), formed at  $z_{\text{ini}} \lesssim 20$ – $40$ , produce a stochastic background in the frequency range  $\sim 10$  Hz– $5$  kHz. In particular, the GW spectra peak at  $\nu_{\text{obs}} \approx 200$  Hz. If the black hole population forms at low redshifts (e.g.  $z_{\text{ini}} \lesssim 10$ ), both the frequency where  $\Omega_{\text{GW}}$  peaks and the minimum frequency of the spectra will be shifted to greater frequencies than those presented here.

However, the shape of  $\Omega_{\text{GW}}$  does not considerably change if we consider the same GW energy power spectrum for the sources. On the other hand, more massive stars ( $m > 200 M_{\odot}$ ) will shifted the peak of the spectra for low frequencies. See for a moment the results of Marassi, Schneider & Ferrari (2009) for black hole remnants

of Population III stars with masses  $100\text{--}500 M_{\odot}$ . Their spectrum peaks at  $\nu_{\text{obs}} = 2.74 \text{ Hz}$  ( $\Omega_{\text{GW}} \approx 5 \times 10^{-15}$ ) and the maximum frequency of the background is  $\sim 600 \text{ Hz}$ .

Another example can be seen from the work of Buonanno et al. (2005). The authors studied the GWB from all cosmic supernovae. Their fiducial model peaks at  $\nu_{\text{obs}} = 6 \text{ Hz}$  ( $\Omega_{\text{GW}} \approx 10^{-13}$ ) while the maximum frequency of the background is  $\sim 3 \text{ kHz}$  and the spectrum can extend to very low frequencies ( $\nu_{\text{obs}} \lesssim 10^{-4} \text{ Hz}$ ). Thus, in principle, it would be possible to identify the signatures of different backgrounds if we have the curve  $\Omega_{\text{GW}}$  versus  $\nu_{\text{obs}}$  over a large range in frequency.

Last but not least, we refer the reader to the work of Kauffmann & Haehnelt (2000) who present a unified model for the evolution of galaxies and quasars. Specifically, these authors discuss that gas cooling is not efficient in too massive structures and so haloes with circular velocity greater than  $600 \text{ km s}^{-1}$  could not form stars. If we take into account their results then the upper limit,  $M_{\text{max}}$ , in equation (10) should be changed for  $\sim 10^{13} M_{\odot}$ .

We checked all the models described in Tables 1–3 with this new upper limit ( $M_{\text{max}} = 10^{13} M_{\odot}$ ). We verify that the amplitude of the CSFR decreases slightly at  $z \lesssim 3.5$  when compared with the results obtained using  $M_{\text{max}} = 10^{18} M_{\odot}$  (at  $z > 3.5$  we do not observe any modification in the behaviour of  $\dot{\rho}_{\star}$ ). For the models with  $M_{\text{min}} = 10^6 M_{\odot}$  ( $10^8 M_{\odot}$ ) there is only a subtle modification in the final results. In particular, the S/N are  $\sim 3.9$  per cent ( $\sim 4.6$  per cent) lower than those presented in Table 1 (2). For the models with  $M_{\text{min}} = 10^{10} M_{\odot}$  we note a modification  $\sim 8.6$  per cent in the results of the Table 3. However, all models presented in Tables 1–3 satisfy the ‘two criteria’, as discussed in Section 4. That is, same using  $M_{\text{max}} = 10^{13} M_{\odot}$  the models produce  $S/N > 3$  and  $\chi_{\tau} \leq 1$ .

## ACKNOWLEDGMENTS

ESP and ODM thank Cláudia V. Rodrigues, Ronaldo E. de Souza, José C. N. de Araujo and José A. de Freitas Pacheco for helpful discussions. The authors would like to thank the referee for helpful comments that they feel considerably improved the paper. ESP was financially supported by the Brazilian Agency CAPES, and ODM was partially supported by CNPq (grant 305456/2006-7).

## REFERENCES

- Abel T., Bryan G. L., Norman M. L., 2002, *Sci*, 295, 93  
 Allen B., 1997, in Marck J.-A., Lasota J.-P., eds, *Relativistic Gravitation and Gravitational Radiation*. Cambridge Univ. Press, Princeton, NJ, p. 373  
 Allen B., Romano J. D., 1999, *Phys. Rev. D*, 59, 2001  
 Bardeen J. M., Bond J. R., Kaiser N., Szalay A. S., 1986, *ApJ*, 304, 15  
 Belczynski K., Kalogera V., Bulik T., 2002, *ApJ*, 572, 407  
 Buonanno A., Sigl G., Raffelt G. G., Janka H. T., Müller E., 2005, *Phys. Rev. D*, 72, 084001  
 Carr B. J., 1980, *A&A*, 89, 6  
 Carrol S. M., Press W. H., Turner E. L., 1992, *ARA&A*, 30, 499  
 Chiosi C., Maeder A., 1986, *ARA&A*, 24, 329  
 Christensen N., 1992, *Phys. Rev. D*, 46, 5250  
 Copi C. J., 1997, *ApJ*, 487, 704  
 Daigne F., Olive K. A., Silk J., Stoehr F., Vangioni E., 2006, *ApJ*, 647, 773  
 de Araujo J. C. N., Miranda O. D., 2005, *Phys. Rev. D*, 71, 127503  
 de Araujo J. C. N., Miranda O. D., Aguiar O. D., 2000, *Phys. Rev. D*, 61, 124015  
 de Araujo J. C. N., Miranda O. D., Aguiar O. D., 2002, *MNRAS*, 330, 651  
 de Araujo J. C. N., Miranda O. D., Aguiar O. D., 2004, *MNRAS*, 348, 1373  
 de Freitas Pacheco J. A., 1997, *Astropart. Phys.*, 8, 21  
 Efstathiou G., Bond J. R., White S. D. M., 1992, *MNRAS*, 258, 1p  
 Ellison S., Songaila A., Schaye J., Petinni M., 2000, *AJ*, 120, 1175  
 Ferrari V., Matarrese S., Schneider R., 1999, *MNRAS*, 303, 247  
 Ferrari V., Miniutti G., Pons J. A., 2003, *MNRAS*, 342, 629  
 Flanagan E. E., 1993, *Phys. Rev. D*, 48, 2389  
 Fryer C. L., Woosley S. E., Heger A., 2001, *ApJ*, 550, 372  
 Giovannini M., 2009, preprint (arXiv:0901.3026)  
 Gunn J. E., Peterson B. A., 1965, *ApJ*, 142, 1633  
 Heger A., Woosley S. E., 2002, *ApJ*, 567, 532  
 Hopkins A. M., 2004, *ApJ*, 615, 209  
 Hopkins A. M., 2007, *ApJ*, 654, 1175  
 Hulse R. A., Taylor J. H., 1974, *ApJ*, 191, L59  
 Hulse R. A., Taylor J. H., 1975a, *ApJ*, 195, L51  
 Hulse R. A., Taylor J. H., 1975b, *ApJ*, 201, L55  
 Jenkins A., Frenk C. S., White S. D. M., Colberg J. M., Cole S., Evrard A. E., Couchman H., Yoshida N., 2001, *MNRAS*, 321, 372  
 Kauffmann G., Haehnelt M., 2000, *MNRAS*, 311, 576  
 Kroupa P., 2008, in Knapen J. H., Mahoney T. J., Vazdekis A., eds, *Pathways Through an Eclectic Universe*, ASP Conf. Series 390. Astron. Soc. Pac., San Francisco, p. 3  
 Lukić Z., Heitmann K., Habib S., Bashinsky S., Ricker P. M., 2007, *ApJ*, 671, 1160  
 Maggiore M., 2000, *Phys. Rep.*, 331, 283  
 Marassi S., Schneider R., Ferrari V., 2009, *MNRAS*, 398, 293  
 Miranda O. D., de Araujo J. C. N., Aguiar O. D., 2004, *Classical Quantum Gravity*, 21, S557  
 Peacock J. A., 1999, *Cosmological Physics*. Cambridge Univ. Press, Cambridge  
 Press W. H., Schechter P., 1974, *ApJ*, 193, 425  
 Regimbau T., de Freitas Pacheco J. A., 2006, *ApJ*, 642, 455  
 Salpeter E. E., 1955, *ApJ*, 121, 161  
 Salvadori S., Schneider R., Ferrara A., 2007, *MNRAS*, 381, 647  
 Sandick P., Olive K. A., Daigne F., Vangioni E., 2006, *Phys. Rev. D*, 73, 104024  
 Scalo J., 1986, *Fundamentals Cosmic Phys.*, 11, 1  
 Schmidt M., 1959, *ApJ*, 129, 243  
 Schmidt M., 1963, *ApJ*, 137, 758  
 Sheth R. K., Tormen G., 1999, *MNRAS*, 308, 119  
 Songaila A., Cowie L. L., 1996, *AJ*, 112, 335  
 Springel V., Hernquist L., 2003, *MNRAS*, 339, 312  
 Stark R. F., Piran T., 1986, in Ruffini R., ed., *Proc. Fourth Marcel Grossmann Meeting on General Relativity*. Elsevier Science, Amsterdam, p. 327  
 Suwa Y., Takiwaki T., Kotake K., Sato K., 2007a, *ApJ*, 665, L43  
 Suwa Y., Takiwaki T., Kotake K., Sato K., 2007b, *PASJ*, 59, 771  
 Thorne K. P., 1987, in Hawking S. W., Israel W., eds, *Three Hundred Years of Gravitation*. Cambridge Univ. Press, Cambridge, p. 330  
 Venkatesan A., 2000, *ApJ*, 537, 55  
 Wilkins S. M., Trentham N., Hopkins A. M., 2008, *MNRAS*, 385, 687

This paper has been typeset from a  $\text{\TeX}/\text{\LaTeX}$  file prepared by the author.